

# Size selective trapping and transport of metal nanoparticles near a nanowaveguide

Mark Sadgrove,<sup>\*,†</sup> Takaaki Yoshino,<sup>‡</sup> Masakazu Sugawara,<sup>‡</sup> Yasuyoshi Mitsumori,<sup>‡</sup>  
and Keiichi Edamatsu<sup>‡</sup>

<sup>†</sup>*Department of Physics, Faculty of Science, Tokyo University of Science, 1-3 Kagurazaka,  
Shinjuku-ku, Tokyo 162-8601, Japan*

<sup>‡</sup>*Research Institute of Electrical Communication, Tohoku University, Sendai 980-8577,  
Japan*

E-mail: mark.sadgrove@rs.tus.ac.jp

## Abstract

We demonstrate size selective optical trapping and transport for metal nanoparticles near a nanowaveguide. Using a two-wavelength, counter-propagating mode configuration inside an optical nanofiber, we show that 100 nm diameter and 150 nm diameter gold nanospheres (GNSs) are trapped near the nanofiber center at different optical powers. Conversely, when one nanofiber species is trapped the other may be transported, leading to a sieve like effect. We find good correspondence between our experimental results and numerical simulations of the system.

Filtering particles by size is a requirement across a range of fields including fabrication of artificial quantum emitters,<sup>1–4</sup> detection and separation of biological particles,<sup>5–9</sup> and gas separation.<sup>10</sup> Although mechanical techniques exist for many applications (with some remarkable recent examples <sup>10,11</sup>), in the nanoparticle regime, much recent effort has been

focused on optical methods,<sup>12–14</sup> due to their inherent flexibility. One aspect of optical manipulation showing promise in this area is the use of counterpropagating optical fields, which allows sophisticated particle control including optical pulling type effects and the use of optical nonlinearity to achieve size sensitive optically induced forces.<sup>15,16</sup>

On the other hand, a separate research avenue for the manipulation of nano-size particles of many types makes use of nanostructures including nanowaveguides<sup>17–21</sup> and plasmonic nanostructures.<sup>22,23</sup> In particular, a very recent combination of nanowaveguide techniques with the above-mentioned counter-propagating field method, has led to remarkable selective control of nanodiamonds near to an optical nanofiber conditional on the number of NV centers they contain.<sup>24</sup> This suggests that combining free space and nanooptical manipulation techniques may prove to be fertile ground for selective optical manipulation in a way traditionally confined to atomic systems with narrow resonances.

Here, we apply a technique similar to that pioneered by Fujiwara *et al.*<sup>24</sup> to achieve size selective trapping of gold nanoparticles near a nanowaveguide (an optical nanofiber). In particular, we demonstrate that 150 nm and 100 nm diameter gold nanospheres (GNSs) are optically trapped near the nanofiber surface at different counter-propagating laser powers. Furthermore, in principle when one size of GNS is trapped, the other will be transported, and hence the scheme constitutes a type of optical sieve, operating in the one dimensional (1D) space defined by the nanofiber.

Before presenting our results, we make a brief comparison with other recent size-selective optical sorting schemes. In 2012, Ploschner *et al.*<sup>14</sup> used the evanescent field of counter-propagating 532 nm and 671 nm wavelength beams to separate gold nanoparticles of 100 nm and 150 nm diameter. Here, we use the extra structure imposed by the fiber taper to engineer actual trapping of one species or the other. More recently, in 2018 Nan and Yan<sup>12</sup> used a sophisticated dynamic trapping setup to separate metal nanoparticles with a diameter difference as small as 10 nm. Our simple, static scheme naturally traps one species while transporting the other due to the nanowaveguide mode behavior. These important

differences to previous methods and the simplicity of our technique mean that our scheme is a unique addition to the nanoparticle trapping and sorting toolbox.

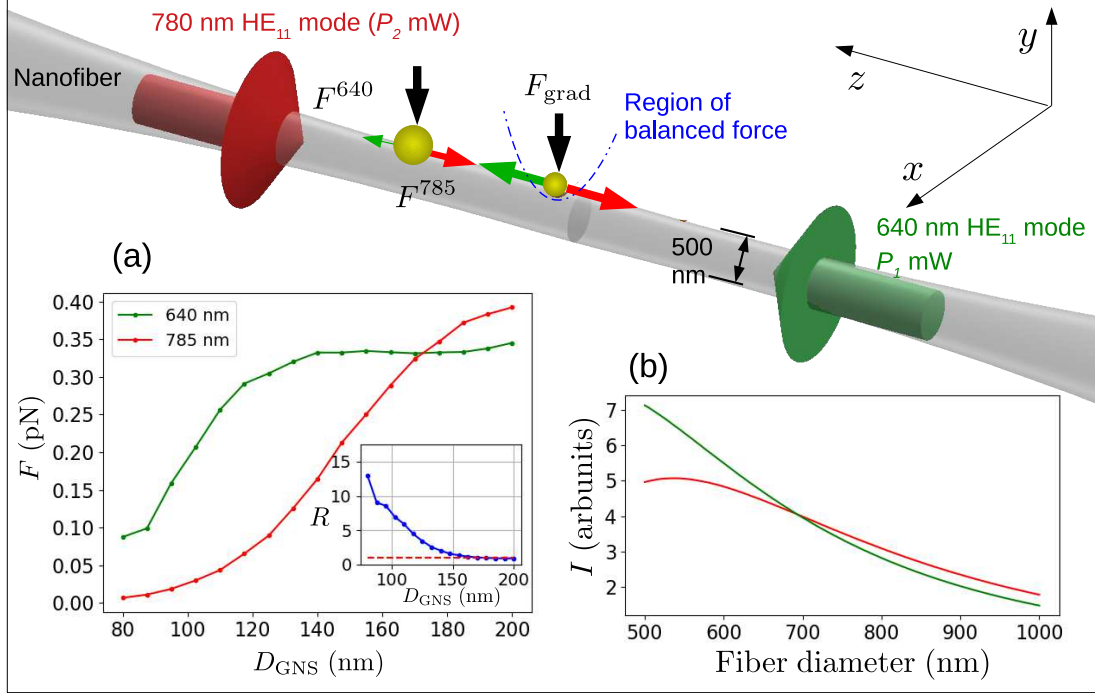


Figure 1: Concept and physical principles. Conceptual diagram showing the trapping and transport of 100 nm and 150 nm diameter gold nanospheres along a 500 nm diameter optical nanofiber. Green and red arrows depict the optical force due to the 640 nm  $HE_{11}$  mode and the 785 nm  $HE_{11}$  mode respectively. Inset (a) shows FDTD simulated force along the fiber axis for 640 nm light and 785 nm light as indicated in the legend, with the inset showing their ratio. Inset (b) shows how the light intensity at the fiber surface depends on the fiber diameter.

The concept of our experiment is illustrated in Fig. 1. Colloidal gold nanospheres (GNSs) which come close to an optical nanofiber are trapped near its surface by the gradient force  $F_{\text{grad}}$  and propelled by the absorption and scattering of photons from the evanescent portion of the fiber mode.<sup>17</sup> This force is  $F^{640}$  in the positive  $z$  direction due to the  $+z$  propagating  $x-$  polarized 640 nm  $HE_{11}$  mode, and  $F^{785}$  in the negative  $z$  direction due to the  $-z$  propagating  $x-$  polarized 785 nm  $HE_{11}$  mode. These forces will balance at a certain power difference between the two beams which depends on the polarizability of the particles at both wavelengths.

Inset (a) of Fig. 1 shows the forces experienced by a particle of diameter  $D_{\text{GNS}}$  on the

surface of a 550 nm diameter nanofiber for an input power of 1 mW at 640 nm wavelength (green points) and 785 nm wavelength (red points). In both cases, the data points show forces evaluated using finite difference time domain (FDTD) simulations of the system for taper parameters matched to experimental values (see Fig. 3(a)), with lines connecting the points to guide the eye. The origin of size selectivity is apparent if we compare the ratio of forces  $R = F^{640}/F^{785}$  at each wavelength as a function of particle size, as shown in the inset. For example, comparing forces on 100 nm and 150 nm diameter particles, we see that  $R \approx 7.5$  and  $R \approx 1.5$  respectively. This means that if we hold the power of the 785 nm mode constant, force balance will occur at a 640 nm mode power which is about five times lower for a 100 nm GNS relative to a 150 nm GNS.

Although the existence of a force balance condition suggests that particles under this condition near the nanofiber center will experience no net force in the  $z$  direction, and thus tend to dwell in that area, they will not be trapped along the  $z$ - axis in a rigorous sense. Nonetheless, in experiments (as explained later) we see that when the power is raised above the force balance condition particles continue to reside near the center of the nanofiber, and exhibit long dwell times implying true trapping. The origin of this behavior may be seen in Inset (b) of Fig. 1 which shows the calculated dependence of the electric field intensity at the nanofiber surface as a function of the fiber diameter for a 640 nm mode (green line) and 785 nm mode (red line). It may be seen that the two curves do not have the same gradient and cross over at a certain fiber diameter. This means that it is possible for the 640 nm mode to exert the dominant force on a particle at one fiber diameter and the 785 nm mode to exert the (oppositely directed) dominant force at a larger diameter. For tapered fibers, this behavior either leads to an unstable potential maximum or a stable (trapping) potential minimum at some point along the taper, with the trap position moving to higher diameter as the power of the 640 nm beam is increased. We refer to this trap configuration as a *two color taper trap* and note that it is distinct from two color trapping at constant nanofiber radius which has been extensively considered, both for atomic systems<sup>25</sup> and for nanoparticles.<sup>19,26</sup>

We will calculate the potential for an explicit example below.

We note that the potentials formed in this way are relatively deep compared to that caused by the radial gradient force, which confines particles to the fiber surface. At the center of the nanofiber, the radial potential depth is about  $60k_B T$ . On the other hand, the taper traps are broad in the  $z$ -direction, giving low trap stiffness.

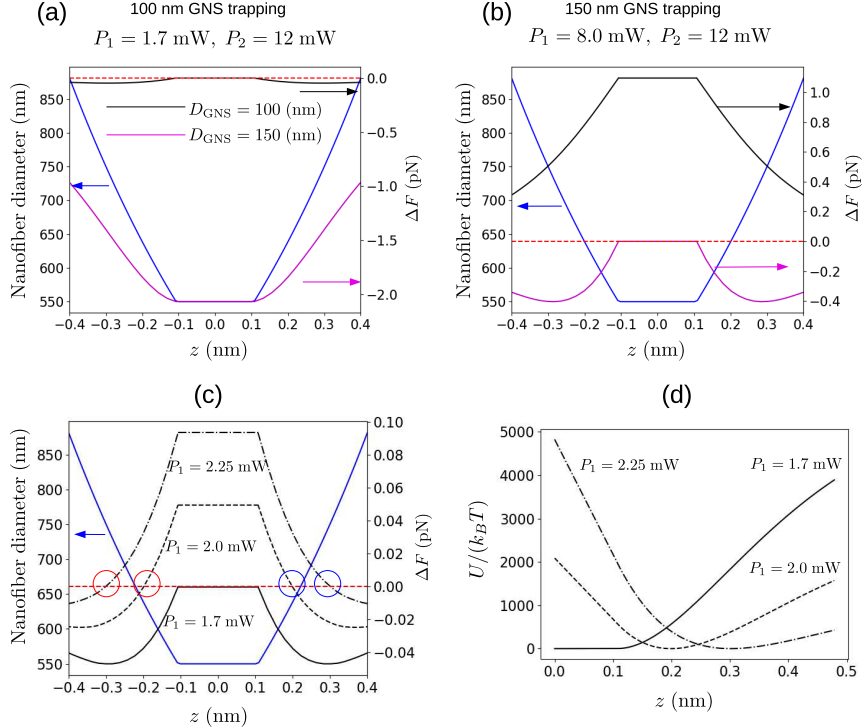


Figure 2: Numerical predictions. (a) and (b) show the dependence of optical forces along the nanofiber axis with  $P_2 = 12$  mW (as in experiments) and given force balance conditions for a 100 nm diameter GNS and a 150 nm diameter GNS respectively. In all cases the blue curve shows the nanofiber taper diameter profile (left hand vertical axis) and black and magenta curves show optical forces on 100 nm and 150 nm diameter GNSs respectively (right hand vertical axis). (c) Variation of the force difference (i.e. total force) on a 100 nm GNS for  $P_1 = 1.5$  mW (force balance condition, solid line),  $P_1 = 1.75$  mW (dashed line) and  $P_1 = 2.0$  mW (dash-dotted line). As before, the blue curve shows the nanofiber taper diameter profile (left hand vertical axis). Blue circles show points where stable trapping is possible, whereas red circles show points where anti-trapping (i.e. a local potential maximum) exists. (d) Shows the potential energy as a function of  $z$  on the positive side of the taper associated with  $P_1 = 1.5$  mW (no trap, solid line),  $P_1 = 1.75$  mW (dashed line), and  $P_1 = 2.0$  mW (dash-dotted line). Note that the potential minimum has been assigned to zero energy in each case to allow simple comparison of the trap depths.

In order to experimentally demonstrate size selective trapping, we chose particles with a

size difference of 50 nm - specifically 100 nm and 150 nm diameter GNSs. This relatively large size difference means that, assuming constant  $P_2$ , trapping occurs for very different  $P_1$  for 100 nm as opposed to 150 nm diameter GNSs. This large power difference allows us to unambiguously identify trapping of the two different particle species, despite the fact that they are below the diffraction limit of our microscope. For smaller particle size differences, it would be necessary to use fluorescently tagged particles with different fluorescence wavelengths in order to confirm size selection, leading to a more complicated experimental setup.

Before moving on to the experiment, we first perform FDTD simulations for the two different particle diameters to determine the likely trapping condition. Figures 2 (a) and (b) show FDTD calculated optical forces  $\Delta F = F^{640} - F^{785}$  for the case of a 100 nm GNS (black line) and a 150 nm GNS (magenta line), with force balance conditions for 100 nm and 150 nm GNSs respectively. The nanofiber diameter is set to 550 nm. With  $P_2$  held at 12 mW, force balance is seen to occur at 1.5 mW in the 640 nm mode for 100 nm diameter GNSs and 7.2 mW in the 640 nm mode for 150 nm diameter GNSs. Figure 2 (c) shows the force  $\Delta F$  on a 100 nm GNS as the power  $P_1$  is raised beyond the force balance condition. It may be seen that the zero crossings of  $\Delta F$  occur at certain positions on the negative and positive  $z$  halves of the taper. On the  $z < 0$  side these zero crossings have an anti-trapping character, where movement away from the zero-force position leads to a growing force in the direction of movement. On the  $z > 0$  side of the taper, the zero-crossings have a trapping character where movement away from the zero position results in a restoring force which pushes the particle back towards the zero position. By numerically integrating the relation  $\Delta F = -\partial U/\partial z$ , where  $U$  is the potential energy of the particle, we can estimate the potential near the zero points for each power in Fig. 2(c). Figure 2(d) shows the results of these calculations. For the case of force balance,  $P_1 = 1.7$  mW (solid line), an inflection point rather than a potential minimum occurs. For  $P = 2.0$  mW and 2.25 mW, a potential minimum is seen at the zero force position, and is seen to move in the positive  $z$  direction

as the power is increased. We have also double checked these calculations using analytical expressions in the Rayleigh approximation. Although the 100 nm diameter GNS is strictly outside the Rayleigh range, we found similar trap depths to those found by integrating the numerically calculated force.

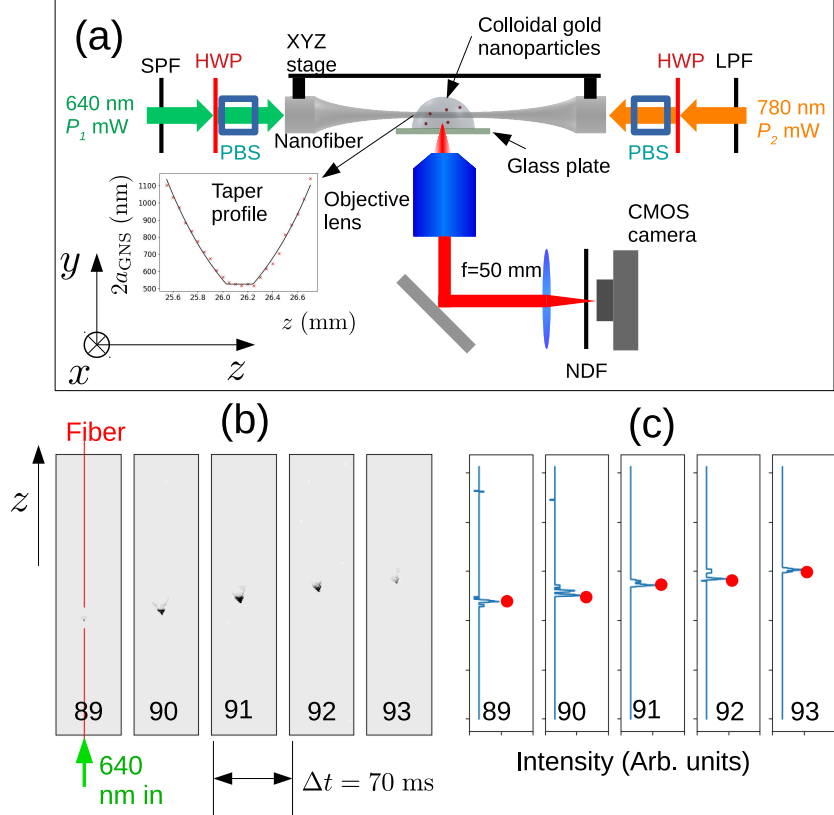


Figure 3: Experiment. (a) The experimental setup. An optical nanofiber was immersed in a droplet containing colloidal gold nanoparticles. Counterpropagating 640 nm and 780 nm wavelength guided modes were introduced into the fiber from diode laser sources, with a short pass filter (SPF) and long pass filter (LPF) employed to keep counterpropagating light from entering the laser diodes. Each field passes through a half-wave plate (HWP) and a polarizing beam splitter (PBS) before entering the fiber. Light scattered from particles trapped by the nanofiber guided modes was collected by an objective lens, attenuated by a neutral density filter (NDF) and detected by a complementary metal-oxide-semiconductor (CMOS) camera. The inset shows the scanning electron microscope measured nanofiber diameter. (b) Example frames from a particle transported along the nanofiber. The frame number is indicated at the bottom of each frame. (c) 1D data extracted from the frames in (b) by taking only the pictures which lie along the fiber line. Red dots indicate peaks, which are detected and used to create a reduced data set. (See text for details).

We now move on to the experiment. The experimental setup is as shown in Fig. 3(a).

An optical nanofiber, with a waist diameter of 550 nm, and waist length of 200  $\mu\text{m}$  was immersed in a droplet of ultra-pure water. Colloidal gold nanoparticles (150 nm diameter: Nanopartz A11-150-CIT-DIH; 100 nm diameter: Nanopartz A11-100-CIT-DIH) were then added to this droplet as necessary. Counterpropagating 640 nm and 780 nm wavelength guided modes were introduced into the fiber from free running diode laser sources, with a short pass filter (SPF) and long pass filter (LPF) employed to keep counterpopagating light from entering the laser diodes. We polarized both fields before they entered the fiber by passing them through a half-wave plate and a polarizing beam splitter, after which the fields were  $x$ -polarized, with an intensity controlled by the half-wave plate angle. Light scattered from particles trapped by the nanofiber guided modes was collected by a 20x objective lens (Olympus LU Plan Fluor, numerical aperture 0.45), attenuated by a neutral density filter (NDF), focused and then detected by a complementary metal-oxide-semiconductor (CMOS) camera (Thorlabs DCC1545M). The CMOS camera measured intensities  $I$  at each pixel constitute our raw data. Example frames are shown in Fig. 3(b), for the situation where  $P_1 = 12$  mW and  $P_2 = 0$  (i.e. no 780 nm mode). The injection direction of the 640 nm laser is shown by the green arrow in the first frame. A trapped, transported particle is seen as a scattering point which moves along the fiber in the same direction as the 640 nm mode. The position of the fiber cannot be clearly seen in the images, due to weak surface scattering, and is marked by a red line in frame 89 of Fig. 3(b). Because the motion is effectively 1D, we can simplify our data considerably by only considering pixels along the line corresponding to the fiber position. Fig. 3(c) shows such 1D data for each frame of Fig. 3(b). The particle is seen as a peak which moves along the  $z$  axis with each consecutive frame.

Our experimental strategy to observe size-selective trapping using the apparatus described above, is to first observe the onset of trapping for a solution containing *only* 150 nm diameter GNSs. Once the power dependence of transport behavior for 150 nm diameter GNSs has been characterized, we add 100 nm diameter colloidal GNSs to the solution and repeat the experiment. Given that the addition of 100 nm GNSs does not alter the trans-

mission properties of the light in the fiber, any observed change in the onset of trapping behavior is attributed to the presence of the 100 nm GNSs.

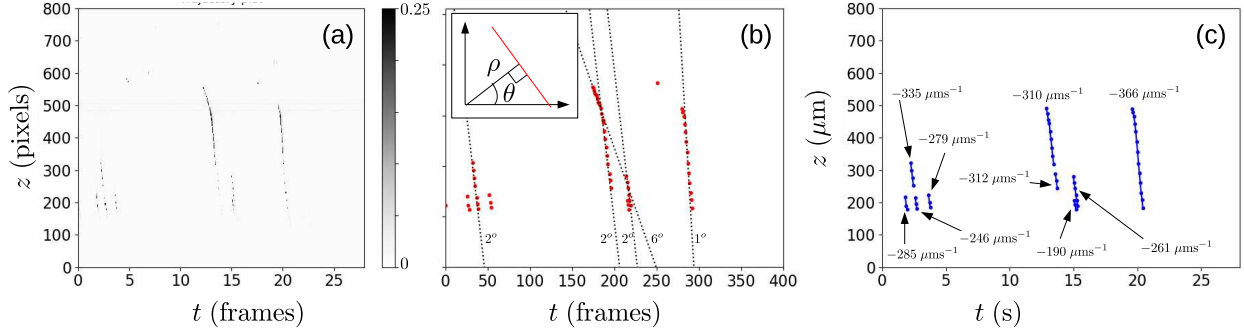


Figure 4: Experimental data: transport of 150 nm diameter GNSs. (a) Combined 1D cross-sections for each captured frame in the data set for parameters  $P_1 = 0$  mW,  $P_2 = 12$  mW, and 150 nm GNSs only. (b) Detected peaks (red points) in 1D cross section data along with five lines detected by a Hough analysis of the data (dashed black lines). The inset depicts the polar representation of a line (shown in red) used by the Hough analysis, and the detected angle  $\theta$  is shown beside each detected line. (c) GNS trajectories detected in the data using the correlation technique explained in the text. The associated mean velocity is shown beside each trajectory.

We now consider our experimental results. First, we consider the case of purely transporting motion for a solution of 150 nm GNSs in the presence of 12 mW of the 780 nm  $HE_{11}$  mode alone. After introducing the fiber to a pure water droplet we added 150 nm GNS producing a concentration of  $2.6 \times 10^5$  particles /  $\mu\text{L}$ . We then took 400 frames of data as an avi file using the CMOS camera. The frames were extracted to individual image files using the *ffmpeg* software program, and a 1D cross-section of each frame was taken along the line corresponding to the fiber position. Combining this 1D data into a single intensity matrix  $I(f, p)$  (where  $f$  is an integer specifying the frame and  $p$  is an integer specifying the pixel) gives Fig. 4(a), where the horizontal axis is the time in frames, and the vertical axis is the distance along the fiber axis in pixels. It is simple to convert the vertical axis to a position in  $\mu\text{m}$  and the horizontal axis to a time in s using a pre-measured calibration factor. Note that in all of our data, the position of the nanofiber center is approximately at the middle of the frame, with an estimated error of  $\pm 100 \mu\text{m}$ .

We then used a peak extraction algorithm (Python Scipy module *find\_peaks*) to find the estimated position of the particle in each frame, resulting in a reduced data set  $(l, m)$  of frame  $l$  and pixel position  $m$  for each detected peak. These positions are shown by red dots in Fig. 4(b). From the peak data, we used two methods to analyze the particle trajectories along the fiber. The first was the Hough-transform method, originally developed for detecting trajectories in bubble chambers, but now commonly used in computer vision problems to detect edges and lines in an image.<sup>27</sup> Using a polar parameterization of a straight line  $(\rho, \theta)$ , as shown in the inset of Fig. 4(b), the Hough transform creates a spectrum of the peak data in  $\rho - \theta$  space. The peaks of the spectrum correspond to lines connecting points in the data, with the largest peak corresponding to the line containing the most points. Sample lines found by the Hough transform are shown as dashed black lines in Fig. 4(b), and their  $\theta$  values are indicated beside each line. The Hough transform can thus provide an *objective estimate* of the most dominant (linear) trajectory in the data.

The second method we used was a simple correlation method to find nearest peaks in consecutive frames. That is, for a given pair  $(l, m)$  in the peak data set, we test whether there exists a pair  $(l + 1, m')$  such that  $t_l < (m - m') < t_u$ , where  $t_l$  and  $t_u$  are lower and upper thresholds chose to minimize false positive detections of trapping trajectories and correlations between unrelated particles respectively. Running the correlation algorithm on the peak data shown in Fig. 4(b) gives the trajectories shown in Fig. 4(c), where the axes have been converted to time in s and distance in  $\mu\text{m}$  by application of the relevant calibration factors. The calculated mean velocity is shown beside each trajectory. We used this method to find the mean and standard deviation of trajectories in each data set.

The use of the above data analysis methods allows us to perform an objective analysis of our data rather than focusing on individual trajectories which are subjectively judged to be of interest.

We now move on to the observation of size selective trapping. First we performed measurements in the presence of 150 nm diameter GNSs only, with the same concentration as

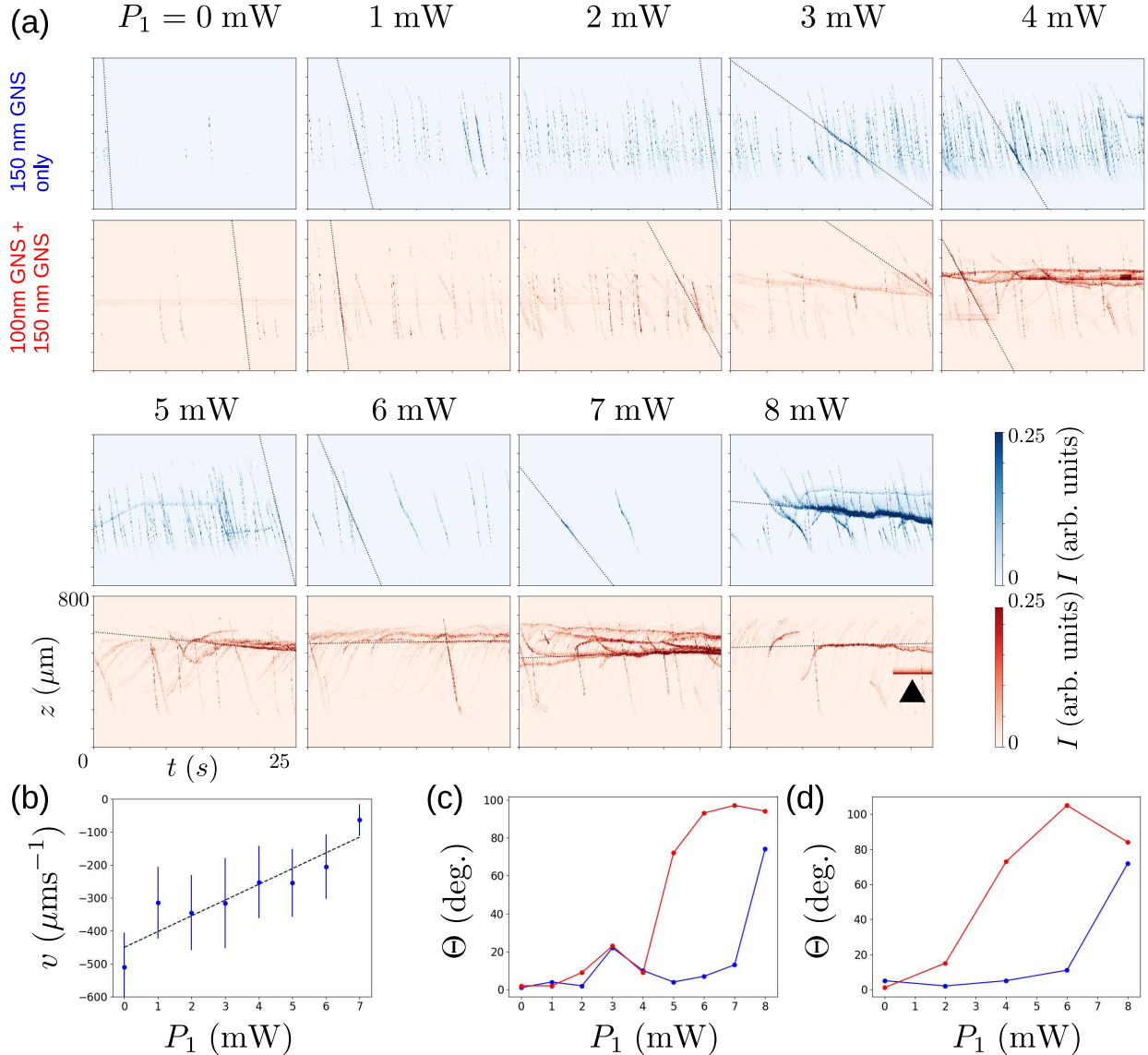


Figure 5: Experimental data: size selective trapping. (a) (Upper rows) Power dependence of transport for 150 nm diameter GNSs, with  $P_1$  as indicated and  $P_2$  fixed at 12 mW. The onset of trapping is observed at  $P_1 = 8$  mW. (Lower rows) Power dependence of transport for a mixture of 100 nm diameter and 150 nm diameter GNSs. The onset of trapping is now observed at  $P_1 = 3$  mW, corresponding to trapping conditions for the 100 nm diameter GNSs. In each case, a black dotted line shows the dominant line of the Hough spectrum. The black arrow in the lower row of the 8 mW data indicates a particle stuck to the fiber surface. This was ignored for the purposes of the Hough analysis. (b) Power dependence of the mean velocity for trajectories detected in each data set shown in the upper rows of (a). Error bars show  $\pm$  one standard deviation. (c) Angle  $\Theta$  of the top ranked line detected by Hough analysis for each data set shown in the upper rows of (a) (blue points) and the bottom row of (a) (red points). (d) Same as (c), but for a data set where there was no control over the polarization of the fields entering the nanofiber.

given above. The power in the 780 nm mode was kept constant at  $P_2 = 12$  mW, while the power of the 640 nm mode was varied from 0 to 8 mW in 1 mW increments. Immediately after setting the power, 400 frames of data was taken. Results are shown in the upper rows of Fig. 5(a). Note that all plots in Fig. 5(a) have the same axes as shown for the  $P_1 = 5$  mW data in the lower row.

Only transporting trajectories in the direction of the 780 nm mode propagation were seen until  $P_1$  reached 8 mW. At this point, trapped particles were observed as can be clearly seen by the near horizontal lines in the combined data  $I(f, p)$ . Note that the onset of trapping occurred near the center of the vertical axis in the constant diameter nanofiber region of the taper as expected from calculations and at the power predicted by FDTD simulation within experimental resolution. The persistent trajectories seen when  $P_1 = 8$  mW are long lived, and show larger intensity than transporting trajectories seen at lower  $P_1$ . The larger intensity is assumed to be due to the presence of multiple trapped particles in the same region. Note that because the force balance only exists near the nanofiber center, at other positions along the taper, transporting trajectories are still seen.

After taking the data shown in the upper row of Fig. 5(a), we added 100 nm diameter GNSs solution to the droplet giving a concentration of  $2.2 \times 10^5$  particles /  $\mu\text{L}$  for the already present 150 nm GNSs and  $6.3 \times 10^5$  particles /  $\mu\text{L}$  for the 100 nm GNSs. No change in the transmitted power of either wavelength mode was observed due to the addition of the solution. We then performed the experiment again at each value of  $P_1$ . This time, the onset of particle trapping occurred at approximately 3 mW, as judged by the appearance of multiple near horizontal particle trajectories (lower row, Fig. 5(a)). Inspection of the data in the lower row of Fig. 5(a) shows interesting behavior beginning at  $P_1 = 5$  mW, where particle trajectories travelling in both directions along the fiber can be seen. For  $P_1 = 8$  mW, the data suggests that many particles travel through the region where other particles are trapped. This is due to 100 nm diameter GNSs being transported along the fiber due to the stronger force they experience from the 640 nm mode. At the same value of  $P_1$  150 nm

GNSs are trapped, and thus the behavior constitutes a type of optical sieve effect, but one where either smaller or larger particles can be retained depending on the adjustable optical parameters.

We note that in the lower row of the 8 mW data, a particle adhering to the fiber is observed. Irreversible particle sticking happened at a rate of approximately once in two hours, and is distinguishable from particle trapping due to the constant position and constant intensity of the scattering observed. The signal due to the adhered particle was ignored for the purposes of the Hough analysis described below.

We also note that although a faint horizontal trajectory can be seen in the 150 nm diameter GNS data at 5 mW, this does not mark the onset of trapping. The reason is that trapping is not seen in the following 6 mW or 7 mW data. Because trapping always exists for a range of powers above the onset power, this rules out 5 mW as the onset of trapping for 150 nm GNSs. Instead the trajectory seen in the 5 mW case is most likely due to a rare smaller diameter particle in the solution.

Although the existence of trapping behavior with different power thresholds can clearly be seen in the raw data shown in Fig. 5(a), a more objective analysis of the transport and trapping behavior can be achieved by using the analysis methods discussed above.

Fig. 5(b) shows the results of a trajectory analysis, and reveals how the mean trajectory velocity reduced to near zero as  $P_1$  was increased. Error bars show plus and minus one standard deviation of the velocity over the observed trajectories. The standard deviation may be seen to be rather large. Variation in the observed velocities is at least partly attributed to the variation in particle size which is specified to be  $\pm 10$  nm.

Fig. 5(c) shows the angle  $\Theta$  at the peak of the Hough spectrum for each data set shown in Fig. 5(a). Note that the dominant line in the Hough spectrum for each data set is shown by a black dotted line in Fig. 5(a). The tendency of this value to  $90^\circ$  with the onset of trapping is a quantitative measure of the fact that in the trapping regime, particle trajectories are dominated by long lifetime trajectories with near-zero velocity. The behavior of  $\Theta$  is clearly

different for the case with only 150 nm diameter GNSs and the case where both 150 nm and 100 nm diameter GNSs are present. We note that the Hough analysis does not conform perfectly with our visual impression of the data. Specifically, although horizontal trajectories indicating trapping are clear in the data for both 3 mW and 4 mW in the case where 100 nm GNSs are present, the Hough analysis for this data detects other lines as dominant in the data. Despite this disagreement with our subjective impression of the data, the Hough analysis is valuable because it provides an objective way of characterizing the data.

We also made similar measurements for a different fiber without polarization control. The Hough angles for these results, shown in Fig. 5(d), show very similar qualitative behavior, suggesting the repeatability of the size-selective trapping behavior. The results also show that polarization control is not necessary to achieve the size-selective trapping effect, which is convenient for practical applications.

Our experimental results reproduce the qualitative aspects of the numerical simulations. In particular 100 nm GNSs are clearly trapped at a lower 640 nm mode power than 150 nm GNSs. Furthermore, powers above the onset of long particle dwell times also result in particle trapping, and the results for  $P_1 = 4, 5$  and 6 mW are suggestive of the the trapping position moving to larger  $z$  values, if not conclusive.

In terms of quantitative agreement, as noted above, for 150 nm GNS trapping a trapping onset of 8 mW was predicted, in agreement with the observed onset power. However, the onset of 100 nm diameter GNS trapping was predicted to occur at 1.7 mW corresponding to 2 mW at the experimental resolution of  $P_1$ . The observed onset was at  $P_1 = 3.0$  mW, up to 150% larger than predicted. At least two reasons for the discrepancies in quantitative agreement in the 100 nm case are readily identified. First, FDTD simulated GNSs do not exhibit an absorption spectrum in agreement with that actually measured. Second, the simulations assume perfect alignment between the linear polarizations of the two modes. Although we arrange the polarizations of the input modes to be linear, and keep the fiber portion leading to the nanofiber straight, optical nanofibers typically have intrinsic birefringence, and so it is

difficult to control the polarization state at the fiber center. We found that the 640 nm light exiting the fiber was still linearly  $x$ –polarized at a level of 99%. Under the same conditions, however, the 780 nm mode showed just 80% linear  $x$ –polarization on exiting the fiber. This is reasonable given the greater penetration depth outside the silica core of the 780 nm mode, and hence it's greater sensitivity to the exact shape of the core.

One obvious question regarding the current method is what the smallest difference in GNS diameters which can be selectively trapped is. In principle the power difference between force balance for two different sized GNSs can be made arbitrarily large by scaling up the powers in each mode. In practice, however, large powers tend to lead to greater sticking of particles to the nanofiber, and heating effects which may disturb the experiment.

It is not possible to give a simple rule for size selectivity due to the non-linearity of  $R$  as seen in Fig. 1(a). For example, if we keep the 780 nm mode power at 12 mW as in the present experiment, and require a power difference of at least 1 mW, between the force balance condition for each particle size, then the selectivity condition may be expressed as  $12|1/R(D_{\text{GNS}}^1) - 1/R(D_{\text{GNS}}^2)| > 1$ . In this case, we find that a 10 nm diameter difference is sufficient for 140 nm and 150 nm diameter GNSs, but for  $D_{\text{GNS}}^1 = 100$  nm diameter, we must increase the particle diameter to  $D_{\text{GNS}}^2 \approx 120$  nm diameter before the condition is satisfied. Furthermore, above about 160 nm,  $R$  saturates, and selective trapping requires much larger powers to reach a desired power gap between balance conditions for two particle species.

Lastly, we note that although the broad qualitative and quantitative features of the size selective method have been demonstrated here, detailed tests of the trapping mechanism would require better control of particle number and more exact identification of the nanofiber center. Given that we have achieved a clear demonstration of the principle here, we leave these details for future investigations.

In conclusion, we have demonstrated a simple method of size-selective trapping for gold nanospheres near the surface of a nanowaveguide. This behavior manifests itself in a power threshold for the onset of trapping which differs strongly depending on particle size. Our

current demonstration was for a 50 nm difference in particle diameters, but simulations suggest that differences at least down to 10 nm are possible. The simplicity and robustness of the experimental setup used here makes it an excellent candidate for practical nanoparticle sorting applications.

## Author information

### Corresponding Author

E-mail: mark.sadgrove@rs.tus.ac.jp

### Author Contributions

M. Sadgrove, conceived of the experiment. M. Sadgrove and T.Y. designed and built the experiment, and contributed to its testing and development. M. Sadgrove gathered the data, performed the analysis, wrote the first version of the paper and co-supervised the experiment. M. Sugawara contributed to fabrication of nanofibers, development and maintenance of the experiment, and discussions regarding the experiment. Y.M. contributed to the development of the experiment and co-supervised the project. K.E. contributed to discussions regarding the experimental data and analysis and co-supervised the project. All authors discussed the manuscript and contributed to manuscript revisions.

## Acknowledgement

M.S. acknowledges support from JSPS KAKENHI (Grant no. JP19H04668) in Scientific Research on Innovative Areas “Nano-material optical-manipulation”.

## Supporting Information Available

### References

- (1) Wang, X.; Zhuang, J.; Peng, Q.; Li, Y. A general strategy for nanocrystal synthesis. *Nature* **2005**, *437*, 121.
- (2) Ryu, S.; Lee, K.; Hong, S. H.; Lee, H. Facile method to sort graphene quantum dots by size through ammonium sulfate addition. *RSC Advances* **2014**, *4*, 56848–56852.
- (3) Wei, J.; Qiu, J.; Ren, L.; Zhang, K.; Wang, S.; Weeks, B. Size sorted multicolor fluorescence graphene oxide quantum dots obtained by differential velocity centrifugation. *Science of Advanced Materials* **2014**, *6*, 1052–1059.
- (4) Morita, Y.; Takimoto, T.; Yamanaka, H.; Kumekawa, K.; Morino, S.; Aonuma, S.; Kimura, T.; Komatsu, N. A Facile and Scalable Process for Size-Controllable Separation of Nanodiamond Particles as Small as 4 nm. *Small* **2008**, *4*, 2154–2157.
- (5) Van Hee, P.; Hoeben, M.; Van der Lans, R.; Van der Wielen, L. Strategy for selection of methods for separation of bioparticles from particle mixtures. *Biotechnology and Bioengineering* **2006**, *94*, 689–709.
- (6) Yeo, J. C.; Wang, Z.; Lim, C. T. Microfluidic size separation of cells and particles using a swinging bucket centrifuge. *Biomicrofluidics* **2015**, *9*, 054114.
- (7) Lin, Q.-Y.; Palacios, E.; Zhou, W.; Li, Z.; Mason, J. A.; Liu, Z.; Lin, H.; Chen, P.-C.; Dravid, V. P.; Aydin, K., et al. DNA-Mediated Size-Selective Nanoparticle Assembly for Multiplexed Surface Encoding. *Nano letters* **2018**, *18*, 2645–2649.
- (8) Xuan, J. Size-based Separation of Bioparticles Using Planar Nanofluidic Devices. **2013**,
- (9) Svoboda, K.; Block, S. M. Biological applications of optical forces. *Annual review of biophysics and biomolecular structure* **1994**, *23*, 247–285.

(10) Carta, M.; Malpass-Evans, R.; Croad, M.; Rogan, Y.; Jansen, J. C.; Bernardo, P.; Bazzarelli, F.; McKeown, N. B. An efficient polymer molecular sieve for membrane gas separations. *Science* **2013**, *339*, 303–307.

(11) Stogin, B. B.; Gockowski, L.; Feldstein, H.; Claure, H.; Wang, J.; Wong, T.-S. Free-standing liquid membranes as unusual particle separators. *Science advances* **2018**, *4*, eaat3276.

(12) Nan, F.; Yan, Z. Sorting Metal Nanoparticles with Dynamic and Tunable Optical Driven Forces. *Nano Letters* **2018**, *18*, 4500–4505.

(13) Righini, M.; Zelenina, A. S.; Girard, C.; Quidant, R. Parallel and selective trapping in a patterned plasmonic landscape. *Nature Physics* **2007**, *3*, 477.

(14) Ploschner, M.; Čižmár, T.; Mazilu, M.; Di Falco, A.; Dholakia, K. Bidirectional Optical Sorting of Gold Nanoparticles. *Nano Letters* **2012**, *12*, 1923–1927, PMID: 22448854.

(15) Kudo, T.; Ishihara, H. Proposed Nonlinear Resonance Laser Technique for Manipulating Nanoparticles. *Phys. Rev. Lett.* **2012**, *109*, 087402.

(16) Wada, T.; Fujiwara, H.; Sasaki, K.; Ishihara, H. Proposed method for highly selective resonant optical manipulation using counter-propagating light waves. *Nanophotonics* **01 Sep. 2020**, *9*, 3335 – 3345.

(17) Kawata, S.; Tani, T. Optically driven Mie particles in an evanescent field along a channeled waveguide. *Optics letters* **1996**, *21*, 1768–1770.

(18) Ng, L.; Luff, B.; Zervas, M.; Wilkinson, J. Propulsion of gold nanoparticles on optical waveguides. *Optics Communications* **2002**, *208*, 117 – 124.

(19) Skelton, S.; Sergides, M.; Patel, R.; Karczewska, E.; Marago, O.; Jones, P. Evanescent wave optical trapping and transport of micro-and nanoparticles on tapered optical

fibers. *Journal of Quantitative Spectroscopy and Radiative Transfer* **2012**, *113*, 2512–2520.

(20) Maimaiti, A.; Truong, V. G.; Sergides, M.; Gusachenko, I.; Chormaic, S. N. Higher order microfibre modes for dielectric particle trapping and propulsion. *Scientific reports* **2015**, *5*, 9077.

(21) Yoshino, T.; Yamaura, D.; Komiya, M.; Sugawara, M.; Mitsumori, Y.; Niwano, M.; Hirano-Iwata, A.; Edamatsu, K.; Sadgrove, M. Optical transport of sub-micron lipid vesicles along a nanofiber. *Opt. Express* **2020**, *28*, 38527–38538.

(22) Tanaka, Y.; Sasaki, K. Optical trapping through the localized surface-plasmon resonance of engineered gold nanoblock pairs. *Optics express* **2011**, *19*, 17462–17468.

(23) Min, C.; Shen, Z.; Shen, J.; Zhang, Y.; Fang, H.; Yuan, G.; Du, L.; Zhu, S.; Lei, T.; Yuan, X. Focused plasmonic trapping of metallic particles. *Nature communications* **2013**, *4*, 2891.

(24) Fujiwara, H.; Yamauchi, K.; Wada, T.; Ishihara, H.; Sasaki, K. Optical selection and sorting of nanoparticles according to quantum mechanical properties. *Science Advances* **2021**, *7*.

(25) Le Kien, F.; Balykin, V. I.; Hakuta, K. Atom trap and waveguide using a two-color evanescent light field around a subwavelength-diameter optical fiber. *Phys. Rev. A* **2004**, *70*, 063403.

(26) Xiao, J. J.; Zheng, H. H.; Sun, Y. X.; Yao, Y. Bipolar optical forces on dielectric and metallic nanoparticles by evanescent wave. *Opt. Lett.* **2010**, *35*, 962–964.

(27) Hough, P. V. Method and means for recognizing complex patterns. 1962; US Patent 3,069,654.